

Camera Calibration for the IceCube Upgrade and Gen2

The IceCube Collaboration

(a complete list of authors can be found at the end of the proceedings)

E-mail: woosik.kang@icecube.wisc.edu, ctoennis@icecube.wisc.edu

An upgrade to the IceCube Neutrino Telescope is currently under construction. For this IceCube Upgrade, seven new strings will be deployed in the central region of the 86 string IceCube detector to enhance the capability to detect neutrinos in the GeV range. One of the main science objectives of the IceCube Upgrade is an improved calibration of the IceCube detector to reduce systematic uncertainties related to the optical properties of the ice. We have developed a novel optical camera and illumination system that will be part of 700 newly developed optical modules to be deployed with the IceCube Upgrade. A combination of transmission and reflection photographic measurements will be used to measure the optical properties of bulk ice between strings and refrozen ice in the drill hole, to determine module positions, and to survey the local ice environments surrounding the sensor module. In this contribution we present the production design, acceptance testing, and plan for post-deployment calibration measurements with the camera system.

Corresponding authors: Woosik Kang^{1*}, Jiwoong Lee¹, Gerrit Roellinghoff¹, Carsten Rott^{1,2}, Christoph Tönnis^{1,3}

¹ *Department of Physics, Sungkyunkwan University, Suwon 16419, Korea*

² *Department of Physics and Astronomy, University of Utah, Salt Lake City, UT 84112, USA*

³ *Institute of Basic Science, Sungkyunkwan University, Suwon 16419, Korea*

* Presenter

37th International Cosmic Ray Conference (ICRC 2021)

July 12th – 23rd, 2021

Online – Berlin, Germany

1. Introduction

Located at the geographic South Pole, the IceCube Neutrino Observatory [1] is the world's largest neutrino telescope in terms of instrumented volume. It consists of a Cherenkov detector of one cubic kilometre volume using the ultra-pure Antarctic ice [2] at depths between 1.45 km and 2.45 km and a square kilometre air-shower detector at the surface of the ice [3]. The primary objectives of the detector are the measurement of high-energy astrophysical neutrino fluxes and determining the sources of these fluxes [4, 5].

Currently an upgrade comprised of seven densely instrumented strings in the centre of the active volume of the IceCube detector with new digital optical modules (DOMs) is being built as the IceCube Upgrade [6]. On each string DOMs will be regularly spaced with a vertical separation of 3 m between depths of 2160 m and 2430 m below the surface of the ice. Three different types of DOMs will be used: The pDOM which is based on the design of the existing IceCube DOMs with upgraded electronics, the D-Egg [7] which has two 8-inch photomultiplier tubes (PMTs) (facing up and down respectively), and the mDOM [8] which has 24 three-inch PMTs distributed for close to uniform directional coverage.

Precise characterization of the optical properties of the IceCube detector medium and thereby reducing uncertainties in directional and energy event reconstruction is one of the goals of the IceCube Upgrade. For this purpose, novel calibration devices will be deployed, with the IceCube Upgrade camera system being a key component.

1.1 Objective and setup of the camera system

The IceCube Upgrade camera system aims to measure the optical properties of the ice in the vicinity of DOMs. Additionally, information on the position and orientation of the optical sensors will be obtained. To do this, the camera system utilises camera modules integrated inside each newly installed DOM to measure light emitted from illumination modules that accompany each camera pointing in the same direction. With this setup, images of both reflected and transmitted light will be taken.

In all three types of new DOMs, three cameras are going to be installed to carry out different types of measurements. In the mDOM two cameras will be installed in the upper hemisphere pointing upwards at 45° . The third camera is positioned at the bottom pole of the mDOM. At the top of the mDOM an additional illumination board is placed to illuminate the refrozen hole ice. In the D-Egg all three cameras are installed on a ring in the lower half of the sensor, point towards the horizon with an angle of 120° to each other. The method of integration into the pDOMs is currently being developed.

In Fig. 1 on the left, one type of measurement is sketched. The downwards facing camera captures direct and scattered light from an illumination module in the DOM below, and the optical properties of the refrozen ice will be inferred based on the distribution of light in the images. Of special interest is a column of ice with different optical properties than the surrounding ice, known as the 'Bubble column', that was originally detected by a special camera system deployed below the deepest DOM of IceCube string 80 [1]. The other cameras on the mDOMs and D-EGGs measure the optical properties of the bulk ice as shown in Fig. 1, right. The bulk ice between strings is illuminated by an LED on one of the DOMs, and a camera in a DOM on a neighboring string takes

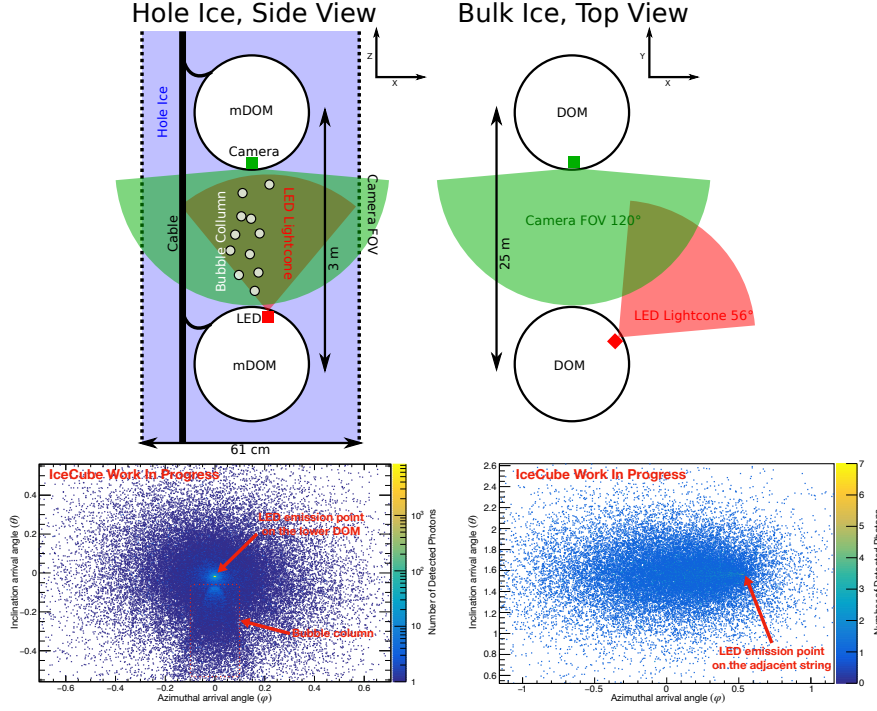


Figure 1: Schematic of planned IceCube Upgrade camera measurements and the simulated images of them. Left: Refrozen hole ice measurement utilising two vertically separated optical modules on the same string. A downward facing camera observes an upward pointing LED from the DOM below. The simulation image in bottom-left represents imaging the bubble column in the refrozen hole ice. Right: Bulk ice measurement utilising two optical modules on separate strings. A camera is observing scattered light from an LED on an adjacent string pointing at an angle of 60° to the camera. The plot in the bottom-right shows the light cone observed from an optical module on the adjacent string in the simulation. The schematic is not to scale. The pixel noise is not included in the simulated images.

images of the scattered light. The optical properties of the ice can be determined based on the distribution of incident light. Since there are multiple cameras pointing in different directions the bulk ice measurement can be performed direction dependent to gauge the anisotropies in the optical properties of the ice [9].

Simulated images based on a photon propagating Monte Carlo code [10] used in previous camera studies [11, 12] are shown in Fig. 1, bottom. The studies are to be extended to develop the image analysis methods which would be applied on the actual image data from the deployed camera system.

1.2 Hardware

The camera module for the IceCube Upgrade camera system is a custom designed device consisting of two PCBs constituting the camera and one PCB that serves as an illumination board. The parts can be seen in Fig. 2. It uses a Sony *IMX225LQR-C* CMOS image sensor, controlled via a Inter Integrated Circuit (I2C) interface with a *MachX02* FPGA by Lattice semiconductor. The FPGA also bridges the incoming communication using a Serial Peripheral Interface (SPI) to the high-speed interface with the image sensor, whose connections to the DOM hardware is shown in

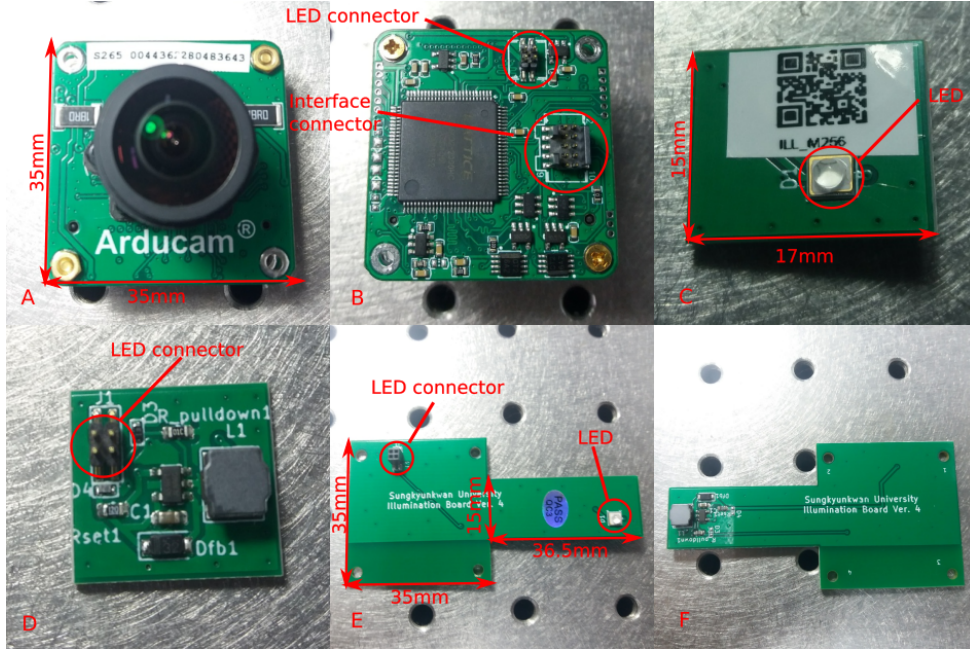


Figure 2: The major components of the IceCube Upgrade camera system. A: The camera as seen from the front; B: The camera as seen from the back showing the connectors for the mainboards and the LED system; C: The LED board for the mDOMs from the front with the LED ID code used to identify the boards; D: The LED board backside that shows the connector; E: The D-EGG illumination system from the front showing the board-to board connector and LED; F: The D-EGG illumination system from the back.

Fig. 3. It also extracts the captured image data from the sensor onto an 8 MB RAM inside the camera that serves as a frame buffer. Images have a maximal resolution of 1312 by 979 pixels with a depth of 12 bits resulting in a file size of 2.7 MB per image using full pixel information, which means that the camera can buffer up to 3 images. The illumination board uses an *SSL 80 GB CS8PM1.13* LED from Oscon. The LED is operated with 1 W of power generating 43 lm of light whose dominant wavelength is 470 nm with the spectral bandwidth of 25 nm. The light emitted has a full width at half maximum of 80°.

Cameras for the mDOM are integrated directly into the 3D-printed PMT holding structure. The cameras look through the glass of the pressure vessel using windows in the holding structure. For the D-EGGs, cameras are attached to rings made from fibre reinforced plastic FR-4 using aluminum brackets. An image of such a ring can be seen in Fig. 4. The rings are glued to the glass of the D-EGG pressure vessels using room temperature vulcanizing silicone glue.

2. Camera calibration and design verification

To verify the camera operation and to calibrate more than 2000 cameras, all the components are subjected to an extensive suite of tests as shown in Fig. 5 (see details in [12]). The entire test cycle for a camera takes 48 hours, with over 3000 (8.1 GB) images captured per camera in the process. During room temperature (20°C) and low temperature (−40°C) tests we capture calibration relevant data for each camera.

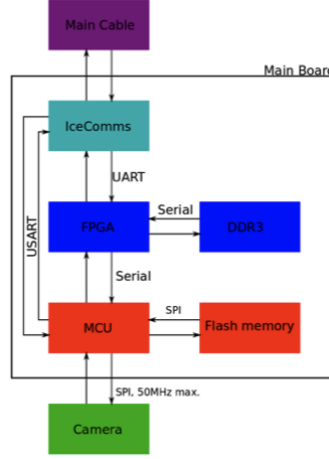


Figure 3: Flow chart of camera data and image transfer speeds between camera and DOM main board.

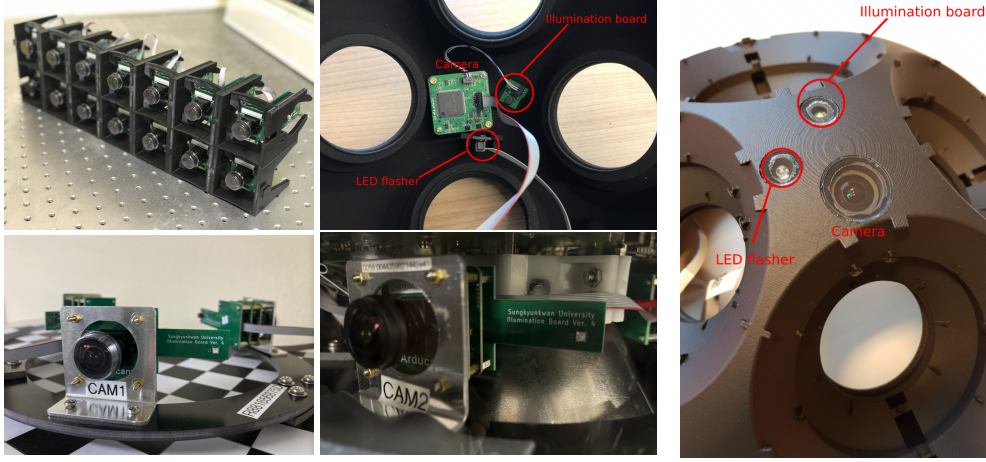


Figure 4: Camera testing battery in custom 3D printed holding docks (top left), assembled camera ring for the D-Egg module with three cameras and illumination boards (bottom left), camera ring integrated in a D-EGG (bottom middle), camera inside a mDOM holding structure (top middle), camera in mDOM holding structure seen from the outside (right)

As cameras will operate in sparse light conditions, a characterization of the pixel darknoise is paramount. Fig. 6 shows the average pixel darknoise at -40°C for different camera settings.

To verify the camera response to a light source, we take multiple images of an LED at a distance of 1 m at different camera settings. Generally, we find that pixel response for unsaturated pixels scales linearly for each camera with exposure time and magnification, which can be expressed in terms of the camera gain as $\sqrt{10^{\text{Gain}[\text{dB}]/10}}$, as shown in Fig. 7. The camera gain is defined as a factor in the conversion of electric charge per pixel to the digital count of that pixel.

We measure the lens - image sensor alignment for each camera (see Fig. 7, right). Manufacturing inaccuracies can result in a small misalignment between the fish-eye lens and image sensor by ~ 0.5 mm. The shift in alignment can be determined with sub pixel accuracy, which translates to an error source for angular estimation below 0.2° .

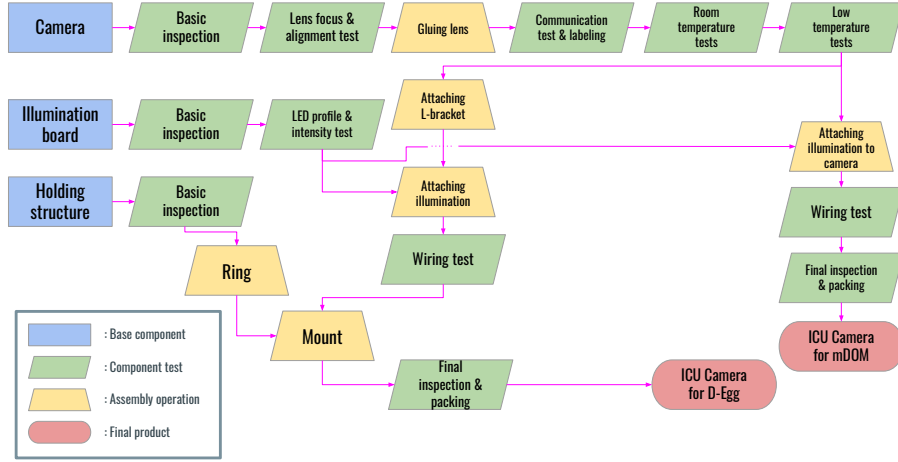


Figure 5: Flow chart for the Camera Acceptance Testing.

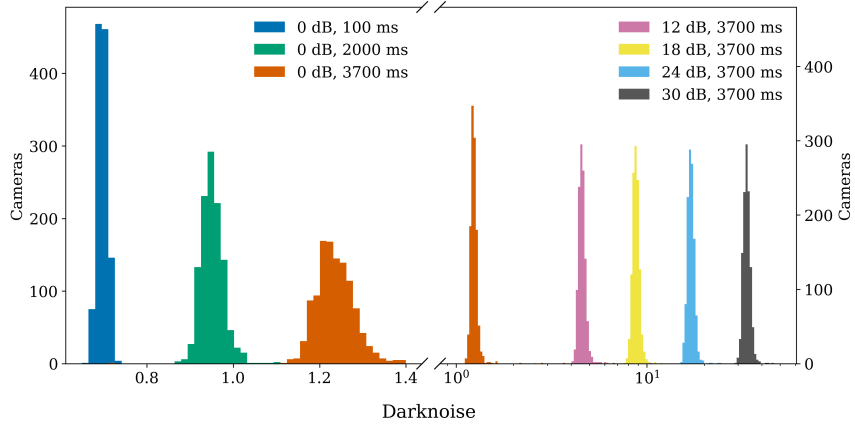


Figure 6: Mean Pixel Darknoise distribution over 1178 cameras for multiple settings

3. Run plans for the camera system and application to IceCube-Gen2

3.1 In-ice run plan of the camera system

To maximize science data taking and to minimize the impact on the detector up-time and on the supernova readiness, camera calibration runs will use a number of approaches; these include keeping the minimal run time required to achieve calibration goals and operating of multiple cameras across the detector simultaneously. Camera runs will require the operation of illumination boards that introduce light in the detector (LID), which will require all optical sensor modules to operate in a calibration mode with the PMT HV switched off. Illumination boards will excite PMTs resulting in an increased noise rate following a calibration run. Fig. 8 shows the increased PMT base rate by switching on the illumination boards and the decrease to normal levels within about 20 min, which is comparable to the settling time of current IceCube detector measured after the runs of the special camera's illumination devices, based on a lab measurement with a 8-inch PMT for D-Egg. Given

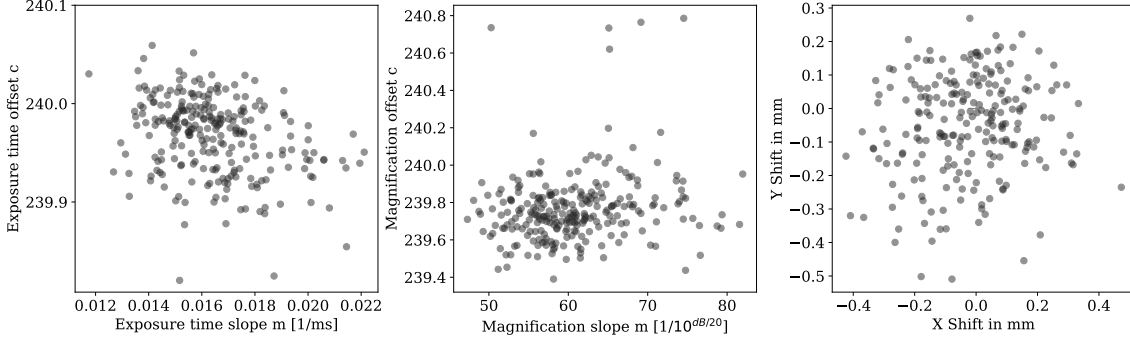


Figure 7: Distribution over 254 cameras, for cameras with R^2 of linear fit to exposure time and magnification better than 0.99. Left: Slope m and offset c for a linear fit to pixel response for increasing exposure time. Middle: Same as left, but linear fit for increasing magnification. Right: Shift between image sensor and lens.

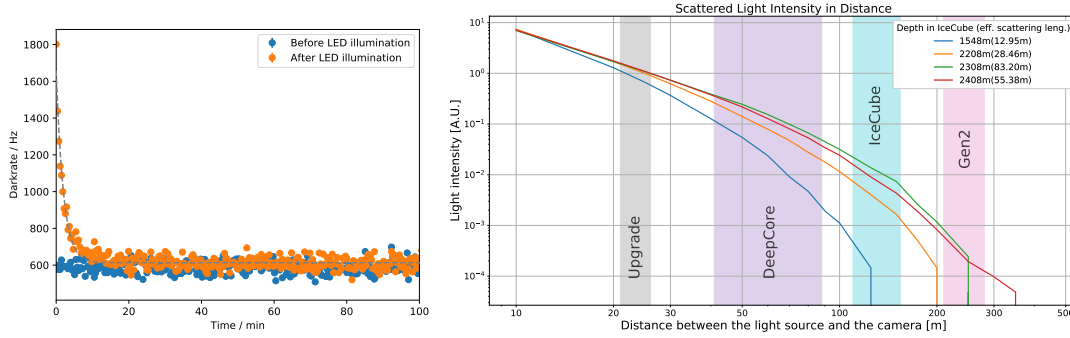


Figure 8: Left: PMT base rate before and after switching on one illumination LED for 90 s. PMT threshold is 0.25 PE. Right: Relative light intensity in cameras directed at an adjacent string with a sideways pointing illumination LED.

the low noise rates at the cold operating temperature of IceCube as well as the operational examples from the current IceCube detector, the impact on nominal detector performance is expected to be minimal. The impact on the supernova trigger can be mitigated by excluding optical modules in the vicinity of the illumination boards that were operated during the calibration run.

A first set of calibration runs cycling through all cameras and all illumination boards, with one camera or LED operating for every second, will be sufficient to triangulate orientations and positions of all DOMs from the observed LEDs in the set of camera images. In-water tests demonstrated that the camera can resolve 10 cm separations at 25 m distance [12]. Once the geometry of each camera is well established, bulk ice measurements can be performed for which a camera observes one or more LEDs on an adjacent string. Hole ice measurements will be performed by operating simultaneously all mDOM - mDOM pairs with the downward facing camera on the upper mDOM taking a transmission photographic image of the illuminated LED in the mDOM below. For reflection photographic hole ice studies a large fraction of all mDOMs will be operated with their bottom camera and the associated LED.

3.2 Application of camera system to the IceCube-Gen2

For IceCube-Gen2 [13] the ice models developed for IceCube can be utilized and a similar camera system base on the experiences for development and operation of the IceCube Upgrade camera system will be employed. The camera system will perform the hole ice related measurements outlined in this work while string to string measurements will be very challenging and are not a priority for Gen2 (see Fig. 8). Bulk ice measurements with cameras could be made via back scattered light using setups similar to those utilised for the SPIceCore camera measurements [14].

4. Conclusions

The camera system is a key component for a comprehensive understanding of the detector medium. Calibration measurements acquired with the IceCube Upgrade act as a science multiplier as they will enable to retroactively analyze more than 15 years of IceCube data with a substantially improved ice model. Improvements in angular and energy resolution directly affect the science capabilities of IceCube. In particular improved neutrino event pointing is critical for multi-messenger science. A significant fraction of cameras have been tested and integrated into the DOMs for the IceCube Upgrade. The evaluated test data demonstrates the quality of the system and its capabilities. For IceCube-Gen2, a similar camera system will be employed to perform a hole ice survey, which also has a potential for bulk ice studies with back scattered light.

References

- [1] **IceCube** Collaboration, M. G. Aartsen *et al.* *JINST* **12** no. 03, (2017) P03012.
- [2] **IceCube** Collaboration, M. G. Aartsen *et al.* *Nucl. Instrum. Meth. A* **711** (2013) 73–89.
- [3] **IceCube** Collaboration, R. Abbasi *et al.* *Nucl. Instrum. Meth. A* **700** (2013) 188–220.
- [4] **IceCube** Collaboration, M. G. Aartsen *et al.* *Science* **342** (2013) 1242856.
- [5] **IceCube** Collaboration, M. G. Aartsen *et al.* *Science* **361** no. 6398, (2018) 147–151.
- [6] **IceCube** Collaboration, A. Ishihara *PoS ICRC2019* (2021) 1031.
- [7] **IceCube** Collaboration, C. Hill *PoS ICRC2021* (these proceedings) 1042.
- [8] **IceCube** Collaboration, L. Classen *PoS ICRC2021* (these proceedings) 1070.
- [9] **IceCube** Collaboration, M. Rongen and D. Chirkin *PoS ICRC2021* (these proceedings) 1119.
- [10] **IceCube** Collaboration, D. Chirkin *Nucl. Instrum. Meth. A* **725** (2013) 141–143.
- [11] **IceCube-Gen2** Collaboration, M. Jeong and W. Kang *PoS ICRC2017* (2018) 1040.
- [12] **IceCube** Collaboration, W. Kang, C. Tönnis, and C. Rott *PoS ICRC2019* (2020) 928.
- [13] **IceCube** Collaboration, A. Karle and M. Kowalski *PoS ICRC2021* (these proceedings) 22.
- [14] **IceCube** Collaboration, D. Kim *PoS ICRC2021* (these proceedings) 1047.

Full Author List: IceCube Collaboration

R. Abbasi¹⁷, M. Ackermann⁵⁹, J. Adams¹⁸, J. A. Aguilar¹², M. Ahlers²², M. Ahrens⁵⁰, C. Alispach²⁸, A. A. Alves Jr.³¹, N. M. Amin⁴², R. An¹⁴, K. Andeen⁴⁰, T. Anderson⁵⁶, G. Anton²⁶, C. Argüelles¹⁴, Y. Ashida³⁸, S. Axani¹⁵, X. Bai⁴⁶, A. Balagopal V.³⁸, A. Barbano²⁸, S. W. Barwick³⁰, B. Bastian⁵⁹, V. Basu³⁸, S. Baur¹², R. Bay⁸, J. J. Beatty^{20,21}, K.-H. Becker⁵⁸, J. Becker Tjus¹¹, C. Bellenghi²⁷, S. BenZvi⁴⁸, D. Berley¹⁹, E. Bernardini^{59,60}, D. Z. Besson^{34,61}, G. Binder^{8,9}, D. Bindig⁵⁸, E. Blaufuss¹⁹, S. Blot⁵⁹, M. Boddenberg¹, F. Bontempo³¹, J. Borowka¹, S. Böser³⁹, O. Botner⁵⁷, J. Böttcher¹, E. Bourbeau²², F. Bradascio⁵⁹, J. Braun³⁸, S. Bron²⁸, J. Brostean-Kaiser⁵⁹, S. Browne³², A. Burgman⁵⁷, R. T. Burley², R. S. Busse⁴¹, M. A. Campana⁴⁵, E. G. Carnie-Bronca², C. Chen⁶, D. Chirkin³⁸, K. Choi⁵², B. A. Clark²⁴, K. Clark³³, L. Classen⁴¹, A. Coleman⁴², G. H. Collin¹⁵, J. M. Conrad¹⁵, P. Coppin¹³, P. Correa¹³, D. F. Cowen^{55,56}, R. Cross⁴⁸, C. Dappen¹, P. Dave⁶, C. De Clercq¹³, J. J. DeLaunay⁵⁶, H. Dembinski⁴², K. Deoskar⁵⁰, S. De Ridder²⁹, A. Desai³⁸, P. Desiati³⁸, K. D. de Vries¹³, G. de Wasseige¹³, M. de With¹⁰, T. DeYoung²⁴, S. Dharani¹, A. Diaz¹⁵, J. C. Díaz-Vélez³⁸, M. Dittmer⁴¹, H. Dujmovic³¹, M. Dunkman⁵⁶, M. A. DuVernois³⁸, E. Dvorak⁴⁶, T. Ehrhardt³⁹, P. Eller²⁷, R. Engel^{31,32}, H. Erpenbeck¹, J. Evans¹⁹, P. A. Evenson⁴², K. L. Fan¹⁹, A. R. Fazely⁷, S. Fiedlschuster²⁶, A. T. Fienberg⁵⁶, K. Filimonov⁸, C. Finley⁵⁰, L. Fischer⁵⁹, D. Fox⁵⁵, A. Frankowski^{11,59}, E. Friedman¹⁹, A. Fritz³⁹, P. Fürst¹, T. K. Gaisser⁴², J. Gallagher³⁷, E. Ganster¹, A. Garcia¹⁴, S. Garrappa⁵⁹, L. Gerhardt⁹, A. Ghadimi⁵⁴, C. Glaser⁵⁷, T. Glauch²⁷, T. Glüsenskamp²⁶, A. Goldschmidt⁹, J. G. Gonzalez⁴², S. Goswami⁵⁴, D. Grant²⁴, T. Grégoire⁵⁶, S. Griswold⁴⁸, M. Gündüz¹¹, C. Günther¹, C. Haack²⁷, A. Hallgren⁵⁷, R. Halliday²⁴, L. Halve¹, F. Halzen³⁸, M. Ha Minh²⁷, K. Hanson³⁸, J. Hardin³⁸, A. A. Harnisch²⁴, A. Haungs³¹, S. Hauser¹, D. Hebecker¹⁰, K. Helbing⁵⁸, F. Henningsen²⁷, E. C. Hettinger²⁴, S. Hickford⁵⁸, J. Hignight²⁵, C. Hill¹⁶, G. C. Hill², K. D. Hoffman¹⁹, R. Hoffmann⁵⁸, T. Hoinka²³, B. Hokanson-Fasig³⁸, K. Hoshina^{38,62}, F. Huang⁵⁶, M. Huber²⁷, T. Huber³¹, K. Hultqvist⁵⁰, M. Hünnefeld²³, R. Hussain³⁸, S. In⁵², N. Iovine¹², A. Ishihara¹⁶, M. Jansson⁵⁰, G. S. Japaridze⁵, M. Jeong⁵², B. J. P. Jones⁴, D. Kang³¹, W. Kang⁵², X. Kang⁴⁵, A. Kappes⁴¹, D. Kappesser³⁹, T. Karg⁵⁹, M. Kar²⁷, A. Karle³⁸, U. Katz²⁶, M. Kauer³⁸, M. Kellermann¹, J. L. Kelley³⁸, A. Kheirandish⁵⁶, K. Kin¹⁶, T. Kintscher⁵⁹, J. Kiryluk⁵¹, S. R. Klein^{8,9}, R. Koirala⁴², H. Kolanoski¹⁰, T. Kontrimas²⁷, L. Köpke³⁹, C. Kopper²⁴, S. Kopper⁵⁴, D. J. Koskinen²², P. Koundal³¹, M. Kovacevich⁴⁵, M. Kowalski^{10,59}, T. Kozynets²², E. Kun¹¹, N. Kurahashi⁴⁵, N. Lad⁵⁹, C. Lagunas Gualda⁵⁹, J. L. Lanfranchi⁵⁶, M. J. Larson¹⁹, F. Lauber⁵⁸, J. P. Lazar^{14,38}, J. W. Lee⁵², K. Leonard³⁸, A. Leszczyńska³², Y. Li⁵⁶, M. Lincetto¹¹, Q. R. Liu³⁸, M. Liubarska²⁵, E. Lohfink³⁹, C. J. Lozano Mariscal⁴¹, L. Lu³⁸, F. Lucarelli²⁸, A. Ludwig^{24,35}, W. Luszczak³⁸, Y. Lyu^{8,9}, W. Y. Ma⁵⁹, J. Madsen³⁸, K. B. M. Mahn²⁴, Y. Makino³⁸, S. Mancina³⁸, I. C. Mariş¹², R. Maruyama⁴³, K. Mase¹⁶, T. McElroy²⁵, F. McNally³⁶, J. V. Mead²², K. Meagher³⁸, A. Medina²¹, M. Meier¹⁶, S. Meighen-Berger²⁷, J. Micallief²⁴, D. Mockler¹², T. Montaruli²⁸, R. W. Moore²⁵, R. Morse³⁸, M. Moulai¹⁵, R. Naab⁵⁹, R. Nagai¹⁶, U. Naumann⁵⁸, J. Necker⁵⁹, L. V. Nguyen²⁴, H. Niederhausen²⁷, M. U. Nisa²⁴, S. C. Nowicki²⁴, D. R. Nygren⁹, A. Obertacke Pollmann⁵⁸, M. Oehler³¹, A. Olivas¹⁹, E. O'Sullivan⁵⁷, H. Pandya⁴², D. V. Pankova⁵⁶, N. Park³³, G. K. Parker⁴, E. N. Paudel⁴², L. Paul⁴⁰, C. Pérez de los Heros⁵⁷, L. Peters¹, J. Peterson³⁸, S. Philippen¹, D. Pieloth²³, S. Pieper⁵⁸, M. Pittermann³², A. Pizzuto³⁸, M. Plum⁴⁰, Y. Popovych³⁹, A. Porcelli²⁹, M. Prado Rodriguez³⁸, P. B. Price⁸, B. Pries²⁴, G. T. Przybylski⁹, C. Raab¹², A. Raisi¹⁸, M. Rameez²², K. Rawlins³, I. C. Rea²⁷, A. Rehman⁴², P. Reichherzer¹¹, R. Reimann¹, G. Renzi¹², E. Resconi²⁷, S. Reusch⁵⁹, W. Rhode²³, M. Richman⁴⁵, B. Riedel³⁸, E. J. Roberts², S. Robertson^{8,9}, G. Roellinghoff⁵², M. Rongen³⁹, C. Rott^{49,52}, T. Ruhe²³, D. Ryckbosch²⁹, D. Rysewyk Cantu²⁴, I. Safa^{14,38}, J. Saffer³², S. E. Sanchez Herrera²⁴, A. Sandrock²³, J. Sandroos³⁹, M. Santander⁵⁴, S. Sarkar⁴⁴, S. Sarkar²⁵, K. Satalecka⁵⁹, M. Scharf¹, M. Schaufel¹, H. Schieler³¹, S. Schindler²⁶, P. Schlunder²³, T. Schmidt¹⁹, A. Schneider³⁸, J. Schneider²⁶, F. G. Schröder^{31,42}, L. Schumacher²⁷, G. Schwefer¹, S. Sclafani⁴⁵, D. Seckel⁴², S. Seunarine⁴⁷, A. Sharma⁵⁷, S. Shefali³², M. Silva³⁸, B. Skrzypek¹⁴, B. Smithers⁴, R. Snihur³⁸, J. Soedingrekso²³, D. Soldin⁴², C. Spannfellner²⁷, G. M. Spiczak⁴⁷, C. Spiering^{59,61}, J. Stachurska⁵⁹, M. Stamatikos²¹, T. Stanev⁴², R. Stein⁵⁹, J. Stettner¹, A. Steuer³⁹, T. Stezelberger⁹, T. Stürwald⁵⁸, T. Stuttard²², G. W. Sullivan¹⁹, I. Taboada⁶, F. Tenholt¹¹, S. Ter-Antonyan⁷, S. Tilav⁴², F. Tischbein¹, K. Tollefson²⁴, L. Tomankova¹¹, C. Tönnis⁵³, S. Toscano¹², D. Tosi³⁸, A. Trettin⁵⁹, M. Tselengidou⁵⁷, C. F. Tung⁶, A. Turcati²⁷, R. Turcotte³¹, C. F. Turley⁵⁶, J. P. Twagirayezu²⁴, B. Ty³⁸, M. A. Unland Elorrieta⁴¹, N. Valtonen-Mattila⁵⁷, J. Vandenbroucke³⁸, N. van Eijndhoven¹³, D. Vannerom¹⁵, J. van Santen⁵⁹, S. Verpoest²⁹, M. Vraeghe²⁹, C. Walck⁵⁰, T. B. Watson⁴, C. Weaver²⁴, P. Weigel¹⁵, A. Weindl³¹, M. J. Weiss⁵⁶, J. Weldert³⁹, C. Wendt³⁸, J. Werthebach²³, M. Weyrauch³², N. Whitehorn^{24,35}, C. H. Wiebusch¹, D. R. Williams⁵⁴, M. Wolf²⁷, K. Woschnagg⁸, G. Wrede²⁶, J. Wulff¹¹, X. W. Xu⁷, Y. Xu⁵¹, J. P. Yanez²⁵, S. Yoshida¹⁶, S. Yu²⁴, T. Yuan³⁸, Z. Zhang⁵¹

¹ III. Physikalisches Institut, RWTH Aachen University, D-52056 Aachen, Germany

² Department of Physics, University of Adelaide, Adelaide, 5005, Australia

³ Dept. of Physics and Astronomy, University of Alaska Anchorage, 3211 Providence Dr., Anchorage, AK 99508, USA

⁴ Dept. of Physics, University of Texas at Arlington, 502 Yates St., Science Hall Rm 108, Box 19059, Arlington, TX 76019, USA

⁵ CTSPPS, Clark-Atlanta University, Atlanta, GA 30314, USA

⁶ School of Physics and Center for Relativistic Astrophysics, Georgia Institute of Technology, Atlanta, GA 30332, USA

⁷ Dept. of Physics, Southern University, Baton Rouge, LA 70813, USA

⁸ Dept. of Physics, University of California, Berkeley, CA 94720, USA

⁹ Lawrence Berkeley National Laboratory, Berkeley, CA 94720, USA

¹⁰ Institut für Physik, Humboldt-Universität zu Berlin, D-12489 Berlin, Germany

¹¹ Fakultät für Physik & Astronomie, Ruhr-Universität Bochum, D-44780 Bochum, Germany

¹² Université Libre de Bruxelles, Science Faculty CP230, B-1050 Brussels, Belgium

¹³ Vrije Universiteit Brussel (VUB), Dienst ELEM, B-1050 Brussels, Belgium

¹⁴ Department of Physics and Laboratory for Particle Physics and Cosmology, Harvard University, Cambridge, MA 02138, USA

¹⁵ Dept. of Physics, Massachusetts Institute of Technology, Cambridge, MA 02139, USA

- ¹⁶ Dept. of Physics and Institute for Global Prominent Research, Chiba University, Chiba 263-8522, Japan
- ¹⁷ Department of Physics, Loyola University Chicago, Chicago, IL 60660, USA
- ¹⁸ Dept. of Physics and Astronomy, University of Canterbury, Private Bag 4800, Christchurch, New Zealand
- ¹⁹ Dept. of Physics, University of Maryland, College Park, MD 20742, USA
- ²⁰ Dept. of Astronomy, Ohio State University, Columbus, OH 43210, USA
- ²¹ Dept. of Physics and Center for Cosmology and Astro-Particle Physics, Ohio State University, Columbus, OH 43210, USA
- ²² Niels Bohr Institute, University of Copenhagen, DK-2100 Copenhagen, Denmark
- ²³ Dept. of Physics, TU Dortmund University, D-44221 Dortmund, Germany
- ²⁴ Dept. of Physics and Astronomy, Michigan State University, East Lansing, MI 48824, USA
- ²⁵ Dept. of Physics, University of Alberta, Edmonton, Alberta, Canada T6G 2E1
- ²⁶ Erlangen Centre for Astroparticle Physics, Friedrich-Alexander-Universität Erlangen-Nürnberg, D-91058 Erlangen, Germany
- ²⁷ Physik-department, Technische Universität München, D-85748 Garching, Germany
- ²⁸ Département de physique nucléaire et corpusculaire, Université de Genève, CH-1211 Genève, Switzerland
- ²⁹ Dept. of Physics and Astronomy, University of Gent, B-9000 Gent, Belgium
- ³⁰ Dept. of Physics and Astronomy, University of California, Irvine, CA 92697, USA
- ³¹ Karlsruhe Institute of Technology, Institute for Astroparticle Physics, D-76021 Karlsruhe, Germany
- ³² Karlsruhe Institute of Technology, Institute of Experimental Particle Physics, D-76021 Karlsruhe, Germany
- ³³ Dept. of Physics, Engineering Physics, and Astronomy, Queen's University, Kingston, ON K7L 3N6, Canada
- ³⁴ Dept. of Physics and Astronomy, University of Kansas, Lawrence, KS 66045, USA
- ³⁵ Department of Physics and Astronomy, UCLA, Los Angeles, CA 90095, USA
- ³⁶ Department of Physics, Mercer University, Macon, GA 31207-0001, USA
- ³⁷ Dept. of Astronomy, University of Wisconsin–Madison, Madison, WI 53706, USA
- ³⁸ Dept. of Physics and Wisconsin IceCube Particle Astrophysics Center, University of Wisconsin–Madison, Madison, WI 53706, USA
- ³⁹ Institute of Physics, University of Mainz, Staudinger Weg 7, D-55099 Mainz, Germany
- ⁴⁰ Department of Physics, Marquette University, Milwaukee, WI, 53201, USA
- ⁴¹ Institut für Kernphysik, Westfälische Wilhelms-Universität Münster, D-48149 Münster, Germany
- ⁴² Bartol Research Institute and Dept. of Physics and Astronomy, University of Delaware, Newark, DE 19716, USA
- ⁴³ Dept. of Physics, Yale University, New Haven, CT 06520, USA
- ⁴⁴ Dept. of Physics, University of Oxford, Parks Road, Oxford OX1 3PU, UK
- ⁴⁵ Dept. of Physics, Drexel University, 3141 Chestnut Street, Philadelphia, PA 19104, USA
- ⁴⁶ Physics Department, South Dakota School of Mines and Technology, Rapid City, SD 57701, USA
- ⁴⁷ Dept. of Physics, University of Wisconsin, River Falls, WI 54022, USA
- ⁴⁸ Dept. of Physics and Astronomy, University of Rochester, Rochester, NY 14627, USA
- ⁴⁹ Department of Physics and Astronomy, University of Utah, Salt Lake City, UT 84112, USA
- ⁵⁰ Oskar Klein Centre and Dept. of Physics, Stockholm University, SE-10691 Stockholm, Sweden
- ⁵¹ Dept. of Physics and Astronomy, Stony Brook University, Stony Brook, NY 11794-3800, USA
- ⁵² Dept. of Physics, Sungkyunkwan University, Suwon 16419, Korea
- ⁵³ Institute of Basic Science, Sungkyunkwan University, Suwon 16419, Korea
- ⁵⁴ Dept. of Physics and Astronomy, University of Alabama, Tuscaloosa, AL 35487, USA
- ⁵⁵ Dept. of Astronomy and Astrophysics, Pennsylvania State University, University Park, PA 16802, USA
- ⁵⁶ Dept. of Physics, Pennsylvania State University, University Park, PA 16802, USA
- ⁵⁷ Dept. of Physics and Astronomy, Uppsala University, Box 516, S-75120 Uppsala, Sweden
- ⁵⁸ Dept. of Physics, University of Wuppertal, D-42119 Wuppertal, Germany
- ⁵⁹ DESY, D-15738 Zeuthen, Germany
- ⁶⁰ Università di Padova, I-35131 Padova, Italy
- ⁶¹ National Research Nuclear University, Moscow Engineering Physics Institute (MEPhI), Moscow 115409, Russia
- ⁶² Earthquake Research Institute, University of Tokyo, Bunkyo, Tokyo 113-0032, Japan

Acknowledgements

USA – U.S. National Science Foundation-Office of Polar Programs, U.S. National Science Foundation-Physics Division, U.S. National Science Foundation-EPSCoR, Wisconsin Alumni Research Foundation, Center for High Throughput Computing (CHTC) at the University of Wisconsin–Madison, Open Science Grid (OSG), Extreme Science and Engineering Discovery Environment (XSEDE), Frontera computing project at the Texas Advanced Computing Center, U.S. Department of Energy-National Energy Research Scientific Computing Center, Particle astrophysics research computing center at the University of Maryland, Institute for Cyber-Enabled Research at Michigan State University, and Astroparticle physics computational facility at Marquette University; Belgium – Funds for Scientific Research (FRS-FNRS and FWO), FWO Odysseus and Big Science programmes, and Belgian Federal Science Policy Office (Belspo); Germany – Bundesministerium für Bildung und Forschung (BMBF), Deutsche Forschungsgemeinschaft (DFG), Helmholtz Alliance for Astroparticle Physics (HAP), Initiative and Networking Fund of the Helmholtz Association, Deutsches Elektronen Synchrotron (DESY), and High Performance Computing cluster of the RWTH Aachen; Sweden – Swedish Research Council, Swedish Polar Research Secretariat, Swedish National Infrastructure for Computing (SNIC), and Knut and Alice Wallenberg Foundation; Australia – Australian

Research Council; Canada – Natural Sciences and Engineering Research Council of Canada, Calcul Québec, Compute Ontario, Canada Foundation for Innovation, WestGrid, and Compute Canada; Denmark – Villum Fonden and Carlsberg Foundation; New Zealand – Marsden Fund; Japan – Japan Society for Promotion of Science (JSPS) and Institute for Global Prominent Research (IGPR) of Chiba University; Korea – National Research Foundation of Korea (NRF); Switzerland – Swiss National Science Foundation (SNSF); United Kingdom – Department of Physics, University of Oxford.